
OPTICAL DESIGN OF A MULTI-OBJECT FIBER-FED SPECTROGRAPH SYSTEM FOR SOUTHERN SPECTROSCOPIC SURVEY TELESCOPE

A PREPRINT

YueFan Shan, ZhengBo Zhu, Hao Tan, Donglin Ma*

School of Optical and Electronic Information and Wuhan National Laboratory of Opto-electronics
Huazhong University of Science and Technology
Wuhan 430074, China
madonglin@hust.edu.cn

February 19, 2021

ABSTRACT

Southern Spectroscopic Survey Telescope (SSST) is a wide-field spectroscopic survey telescope that China plans to build in Chile in the next few years. As an instrument for astronomical spectroscopic survey, the multi-object and fiber-fed spectrograph (MOFFS) is one of the most important scientific instruments for SSST. In this paper, we present a recommended optical design for the MOFFS system based on the Volume Phase Holographic Gratings (VPHG). The whole design philosophy and procedure, including the analytic method to determine the initial structure, optimization procedures of the VPHG and the camera groups, are demonstrated in detail. The numerical results of the final obtained spectrograph show a superior imaging quality and a relatively high transmittance for the whole working waveband and the field of view. The design method proposed in this paper can provide a reference for the design of MOFFS accommodated in spectroscopic survey telescopes.

Keywords Southern Spectroscopic Survey Telescope · spectrograph · Volume Phase Holographic Gratings · Spectroscopic Survey

1 Introduction

Image and spectroscopy are two of the most important observational information in astronomical research. For the former one, a lot of telescopes have been designed for wide-area deep image sky survey observation, such as the Hubble Space Telescope (HST) [1], Large Synoptic Survey Telescope (LSST) [2], Chinese Space Station Telescope (CSST, under construction) [3] and James Webb Space Telescope (JWST, to be launched) [4]. As an indispensable complement, the southern multi-target spectral survey telescope will be the most important and widely used ground-based equipment for the next generation of wide-area image sky survey projects [5]. For the spectroscopy survey, the huge success of Two-Degree Field Galaxy Redshift Survey (2dFGRS) [6] and Sloan Digital Sky Survey (SDSS) [7] have proved that the large-field multi-object spectral survey telescope can maintain competitiveness and efficient scientific output for decades. However, the multi-object spectroscopic survey telescope with an aperture larger than 6 meters and field of view greater than 3 square degrees is a major gap of the parameter space for the current telescopes in service. Therefore, China has planned to build Southern Spectroscopic Survey Telescope (SSST) with an aperture of 6.5 meters and a field of view greater than $2^\circ \times 2^\circ$ in Chile. SSST aims to perform an efficient spectral verification for wide-area image sky survey and reveal the physics behind astronomical events.

Two kinds of recommended optical designs for SSST have been proposed [8, 9], which are designed for the telescope body. But the works about the spectrograph, which is also an important scientific instrument for SSST, have not been reported.

*Shenzhen Huazhong University of Science and Technology, Shenzhen 518057, China

Up to now, the most powerful implemented design of such kind of instruments is the Dark Energy Spectroscopic Instrument (DESI), which was designed for the 3.8-meter Mayall telescope [10]. It has a field of view of 3.2° and can record the spectrum of 5000 different targets at the same time. The working waveband of DESI ranges from 360nm to 980nm. Each spectrograph of DESI consists of three channels and each channel is equipped with a $4k \times 4k$ CCD to obtain the high-resolution spectral information from 500 different objects. However, the statement of the design process was not detailed in [10].

In this paper, we aim to design a multi-object and fiber-fed spectrograph (MOFFS) system with a working waveband ranging from 360nm to 1100nm to cover both near-infrared and visible regions. To make the MOFFS work in a wider spectral range while maintaining a high resolution of spectral imaging, we divide the observing light into four sub-wavebands via 3 dichroic filters. For each sub-waveband, the specific optical channel is elaborately designed respectively, and each channel is equipped with a $4k \times 4k$ CCD with a pixel size of $15\mu\text{m}$. The numerical result shows that the designed optical system has a superior optical performance for spectroscopy measurement.

2 Principle

Figure 1 (a) illustrates the working mechanism of SSST, where light rays coming from the outer space are captured by the telescope firstly, and then these rays enter into one ends of fibers which are located at the focal plane of the telescope. The positions of these fiber's ends on the focal plane can be mechanically adjusted. The other ends of the fibers are mounted linearly forming a so-called fiber slit. Finally, the light rays emitted from the fiber slit are transmitted to the CCD via the spectroscopic imaging system.

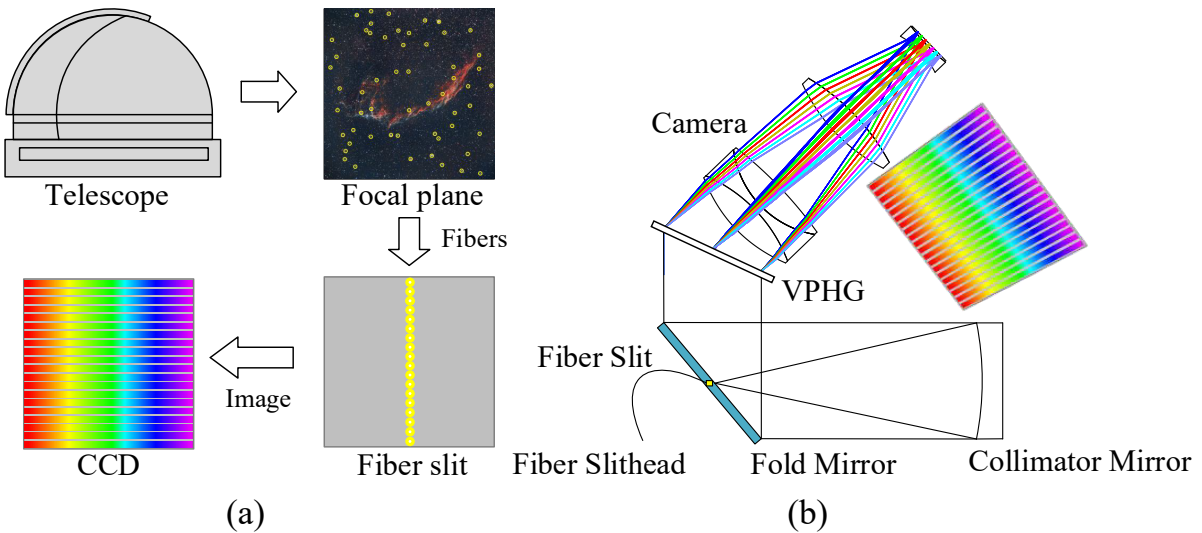


Figure 1: (a) Schematic diagram of SSST; (b) optical layout of one channel of MOFFS.

Figure 1(b) shows the optical layout of one channel of the MOFFS system, which is composed of a fiber slit, a collimator mirror, a folder mirror, a dichroic filter (not drawn), a volume phase holographic grating (VPHG), and a camera unit. The light emitted from the fiber slit is firstly collimated by the collimator mirror. Then the light beam is divided into 4 channels corresponding to 4 sub-wavebands with the help of 3 dichroic filters. After that, the light is dispersed by the VPHG forming the mixed filed of views, and each field of view corresponds to a specific wavelength. Finally, the light beam propagates to CCD via the camera unit. Based on the relevant research experience and the specific application of SSST, we summarize the design technical specifications for the spectrometer optical system in Table 1.

Table 1: Design specification

Wavelength range	360nm - 1100nm
Spectral resolution	$<0.06\text{nm/pixel}$
Transmittance	$>86\%$ (360nm - 390nm) $>90\%$ (390nm - 1100nm)
RMS radius	$15\mu\text{m}$

3 Determination of parameters

3.1 Determination of focal ratio

Focal ratio degradation (FRD) is the most important factor to determine the throughput loss of the Fiber-fed spectrographs [11, 12]. Because of the FRD effect, the divergence angle of the beam emitted from the fiber will be larger than that of the beam entering into the fiber. The light rays beyond the acceptance solid angle of the spectrometer system lead to the FRD loss. So, the magnitude of the FRD effect is greatly determined by the focal ratio of the incident light [13, 14]. According to Lawrence W. Ramsey's study [14], $F/3 \sim F/4$ is the best choice of f-ratio to minimize the FRD effect. As a rule of thumb, we set the f-ratio as $F/3.6$ in our design.

3.2 Determination of Fiber slit's parameters

The fiber slit is the object plane of MOFFS. The parameters of fiber slit are selected according to DESI [10]. The slit length is 120.9mm and contains 500 fibers which are equally spaced, as shown in Fig. 2(a).

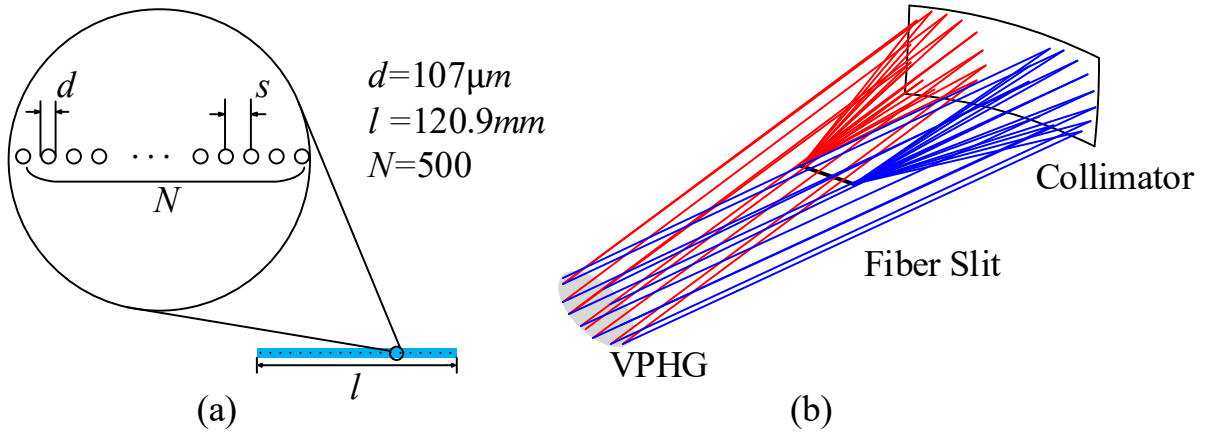


Figure 2: (a) Configuration of the fiber slit; (b) Schematic diagram of collimator system.

3.3 Determination of collimator's parameters

In this design, a single spherical mirror is selected as the collimator as shown in Fig. 2(b). The light rays emanating from both ends of the fiber slit are collimated to be a parallel light beam by the collimator, the angle between these two beams can be approximately calculated as

$$\tan \frac{\theta}{2} = \frac{l}{r}, \quad (1)$$

where θ is the angle between the two beams, l is the length of the fiber slit equaling 120.9mm, and r is the radius of curvature of the collimator mirror. It is clear that the size of the VPHG is determined by the diameter of the collimated parallel beam. A larger collimated beam can definitely guarantee a better optical performance. While large collimated beam means high cost of VPHG. So, a trade-off between the optical performance and the cost of VPHG has to be made. As illustrated in Fig. 3, a larger collimator makes a smaller average RMS radius, i.e. better optical performance. When the diameter of the collimator increases to 170mm, the descent rate of the average RMS radius tended to be an uneconomical level. So, we choose the diameter of collimator as 170mm in this design.

The radius of curvature of the collimator mirror can be obtained as follows

$$F/\# \cdot D = \frac{r}{2} \quad (2)$$

where $F/\#$ is the focal ratio of the beam emitted from the fiber slit, D is the diameter of the collimator mirror. As mentioned above, $F/\#$ is 3.6 and D is 170mm. So, we can get $r=1224$ mm and $\theta \approx 11.28^\circ$. As a result, the distance from the fiber slit to the collimator mirror can be calculated as $D \cdot F/\# = 612$ mm.

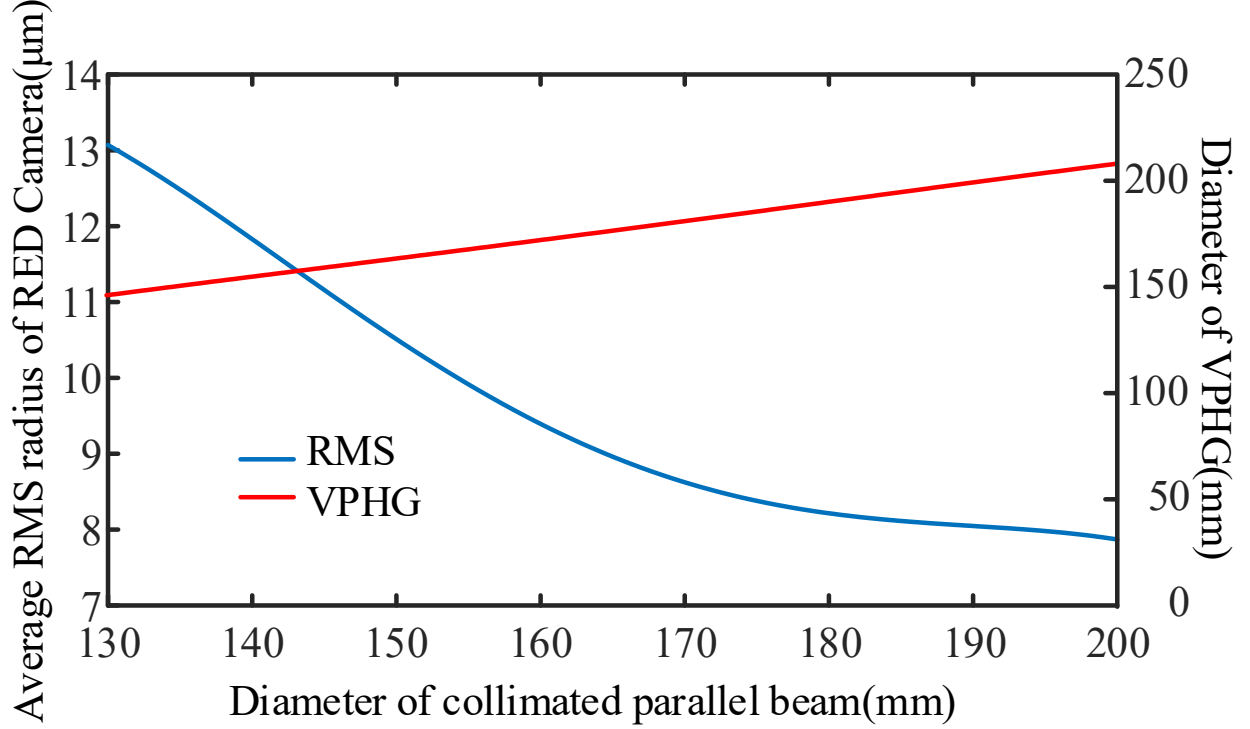


Figure 3: Average RMS radius of RED Camera Vs diameter of collimated beam.

3.4 Determination of dichroic's parameters

For the waveband ranging from λ_1 to λ_2 , the average spectral resolution can be approximately expressed as

$$\Delta\lambda = \frac{(\lambda_2 - \lambda_1)}{N}, \quad (3)$$

where N is the number of pixels along the x or y direction of CCD. Considering the requirement of spectral resolution, we divide the whole waveband into four channels as listed in Table 2. The layout of the whole optical system is illustrated in Fig. 4, and the corresponding parameters of the 3 dichroics are listed in Table 3.

Table 2: Waveband for each channel.

Channel	Wavelength range
BLUE	360nm-580nm
RED	560nm-740nm
NIR	720nm-900nm
IR	877nm-1100nm

Table 3: Parameter requirements of dichroics.

Dichroic	RED Pass	NIR and IR Pass	IR Pass
Transmission Band	580nm-740nm	740nm-1100nm	900nm-1100nm
Reflection Band	360nm -560nm	360nm -720nm	360nm -877nm
Crossover Region	560nm -580nm	720nm -740nm	877nm -900nm
Crossover Width	20nm	20nm	22.5nm

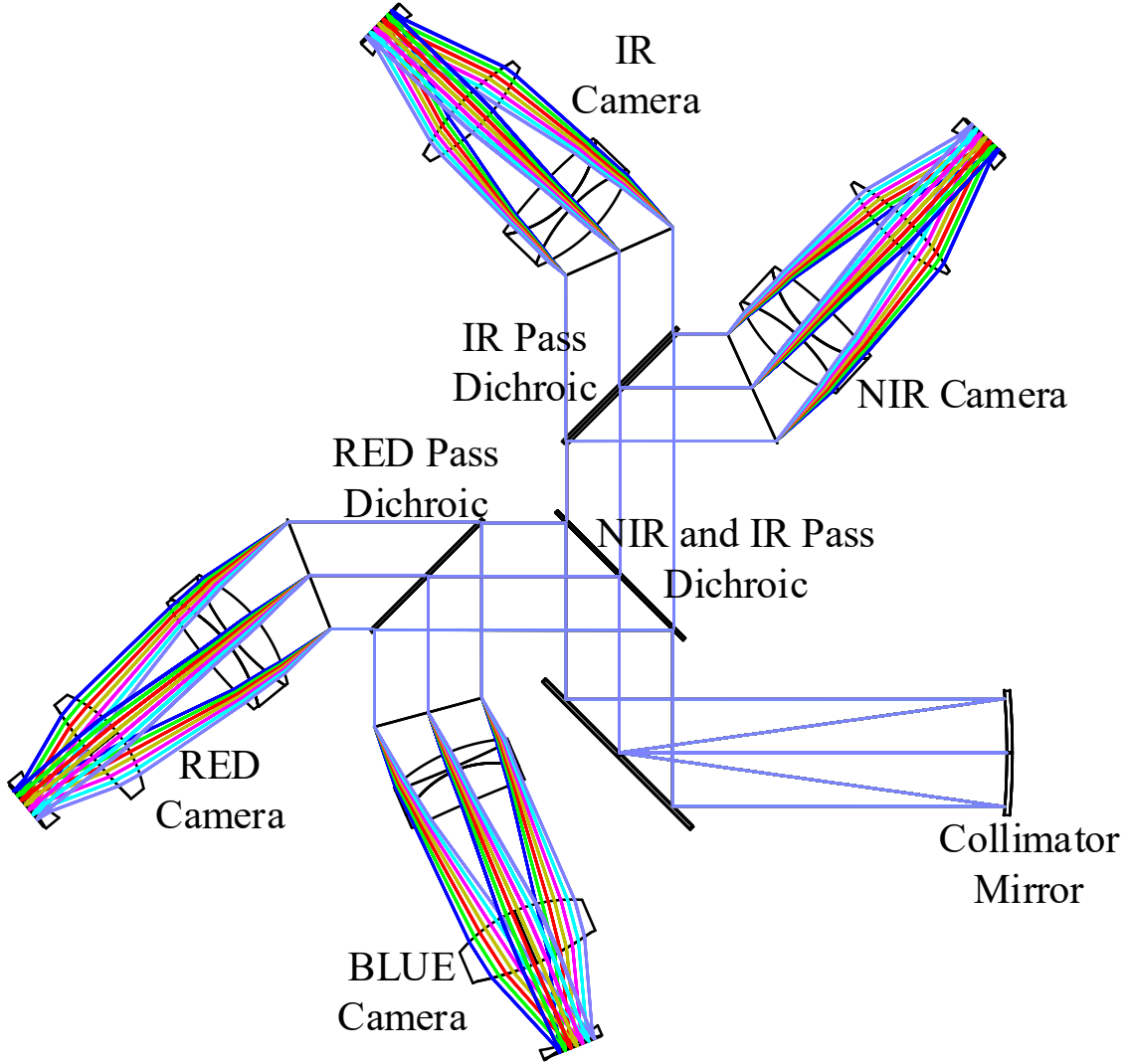


Figure 4: Design layout of the whole system of multi-object fiber-fed spectrographs.

3.5 Determination of VPHG's parameters

Figure 5(a) detailedly shows the optical layout of one of the four channels of the spectrometer. VPHG is the kernel optical element of the whole system dispersing the incident light into different angles for the different wavelength of light.

Supposing that the diffraction angles β_1 and β_2 are for the light with a shorter wavelength λ_1 and the longer wavelength λ_2 , respectively. Their relation can be specified as

$$\begin{cases} d(\sin \beta_1 + \sin i) = k \cdot \lambda_1 \\ d(\sin \beta_2 + \sin i) = k \cdot \lambda_2 \end{cases}, \quad (4)$$

where d is the grating period, i donates the incident angle and k represents the diffraction order. The divergence angle $\Delta\beta$ of the dispersed beam can be calculated as

$$\Delta\beta = \beta_2 - \beta_1 = \arcsin\left(\frac{k \cdot \lambda_2}{d} - \sin i\right) - \arcsin\left(\frac{k \cdot \lambda_1}{d} - \sin i\right). \quad (5)$$

In this design, only +1 diffraction order is considered, which means that $k = 1$ in Eq. (5). Since the initial structure of the camera group lens of the spectrometer is rotationally symmetrical about the optical axis, the dispersion angle

can be approximated to the field of view of the camera group, which means $\Delta\beta \approx \theta$. The line density of VPHG for each channel is determined based on the conventional choice [10, 15], the incident angle and dispersion angle are also calculated as listed in Table 4. These parameters are the basis to determine the initial optical structure of the spectrometer.

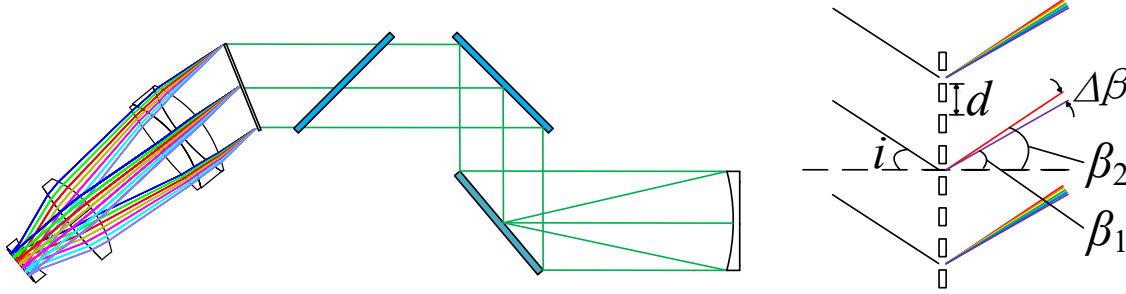


Figure 5: (a) Design layout of one channel of MOFFS; (b) Schematic diagram of grating's dispersion effect.

Table 4: **Initial parameters of the VPHG.**

Channel	BLUE	RED	NIR	IR
Wavelength range	360nm-580nm	560nm-740nm	720nm-900nm	877nm-1100nm
Linear density	900 lines/mm	1050 lines/mm	1000 lines/mm	850 lines/mm
Incident angle	25.05°	24.11°	24.2°	34.67°
Grating spectral dispersion	11.3632°	11.2825°	11.2818°	11.2819°

3.6 Determination of camera group's parameters

The size of the photosensitive region of 4K×4K CCD equals 61.44mm×61.44mm. Taking the alignment tolerance and edge effects of CCD into consideration [10], only the central region of 59mm×59mm is considered. The focal length of the camera group can be obtained as

$$f = a \left(2 \tan \frac{\theta}{2} \right)^{-1}, \quad (6)$$

where a is the margin length of the working area of CCD. With the information given above, the value of f is calculated as 298.66mm.

4 Design and results

4.1 Optical layout of the system

As shown in Fig. 6, the fiber slit is positioned at the optical axis of the spherical collimator mirror. To avoid the vignetting effect caused by the fiber slit as well as the fiber bundle, a flat fold mirror is located physically around the fiber slit. The reflected beam is divided into 4 channels by the 3 dichroics. Since most glasses have a strong spectral absorption around 360nm, the blue channel is designed as a reflective unit before the camera group lens.

4.2 Design procedures

The initial optical structure of the camera group optical system is determined by the focal length and the field angle that have been provided in Eq. (1) and Eq. (6). The optical performance requirements for the camera groups are listed in Table 5.

Firstly, we choose the Petzval lens system as the initial structure as shown in Fig. 7(a), which consists of two positive lenses [16, 17]. The power of the whole optical system is equally distributed in two lenses. And, a field flattener is usually added near the image plane to improve the optical performance as shown in Fig. 7(b) [18]. To further simplify the design, our design is promoted to have a triplet lens, a single positive lens, and a field flattener as shown in Fig. 8(a).

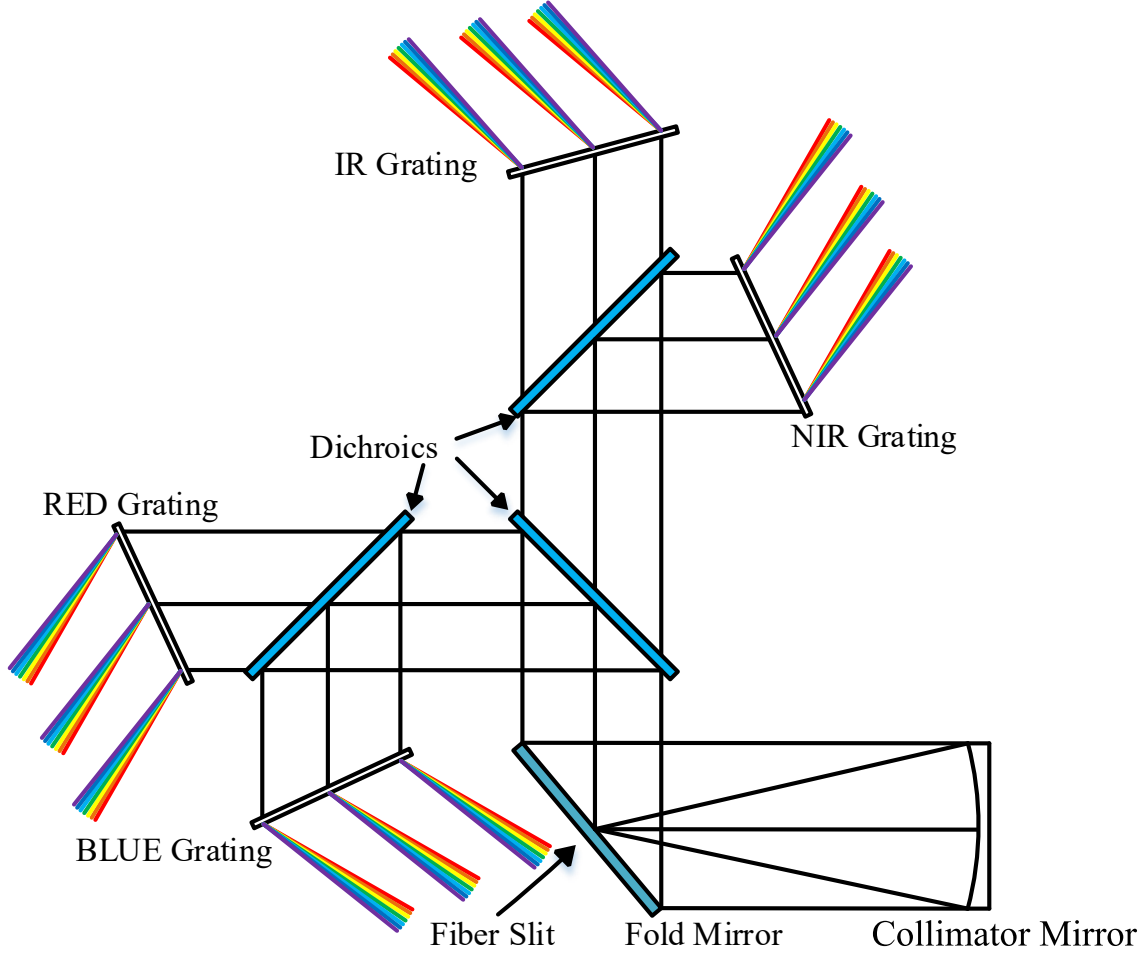


Figure 6: Design layout of optical arrangement.

Table 5: Parameter requirements of the camera group lens.

Channel	BLUE	RED	NIR	IR
Wavelength range	360nm-580nm	560nm-740nm	720nm-900nm	877nm-1100nm
Spectral resolution	< 0.057nm/pixel	< 0.052nm/pixel	< 0.052nm/pixel	< 0.057nm/pixel
Transmittance	> 86%(360nm – 390nm) > 90%(390nm – 580nm)	> 90%	> 90%	> 90%
RMS radius	<13 μ m	<13 μ m	<13 μ m	<13 μ m
Focal length	298.66mm	298.66mm	298.66mm	298.66mm

To correct the field curvature introduced by the collimator mirror, we use a “biconical” surface as the front surface of the field flattener as shown in Fig. 8(b). The sag height of the biconical surface is expressed as

$$z = \frac{c_x x^2 + c_y y^2}{1 + \sqrt{1 - (1 + k_x) c_x^2 x^2 - (1 + k_y) c_y^2 y^2}}, \quad (7)$$

where c_x and c_y are curvatures of the surface in x and y directions, and k_x and k_y are the conic coefficients of the surface in x and y directions. Considering the cost, the spectral absorption characteristics, the refractive index, and the Abbe number, the selected glass combinations for each channel are listed in Table 6. Since most glasses have strong absorption for the blue spectrum, the transmittance plays a major role in the glass choice in the BLUE channel. The main reason for choosing fused silica as the material of the last lens is that it is not radioactive [10]. After the initial structure of the camera group, the VPHG and the collimator mirrors are independently designed, and then we take a

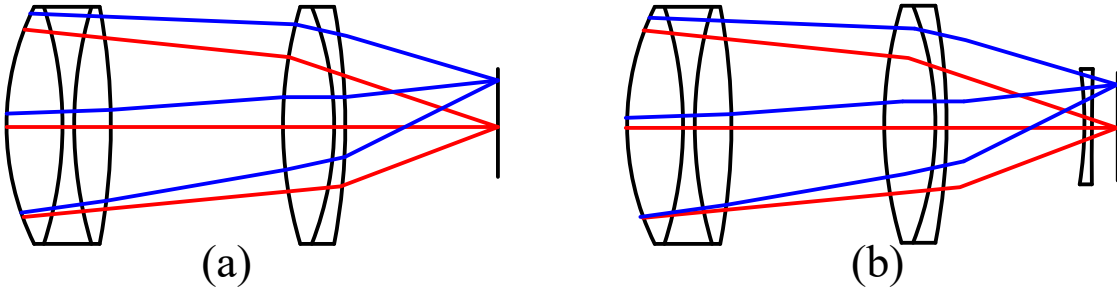


Figure 7: Evolution of the initial structure model for the camera group.

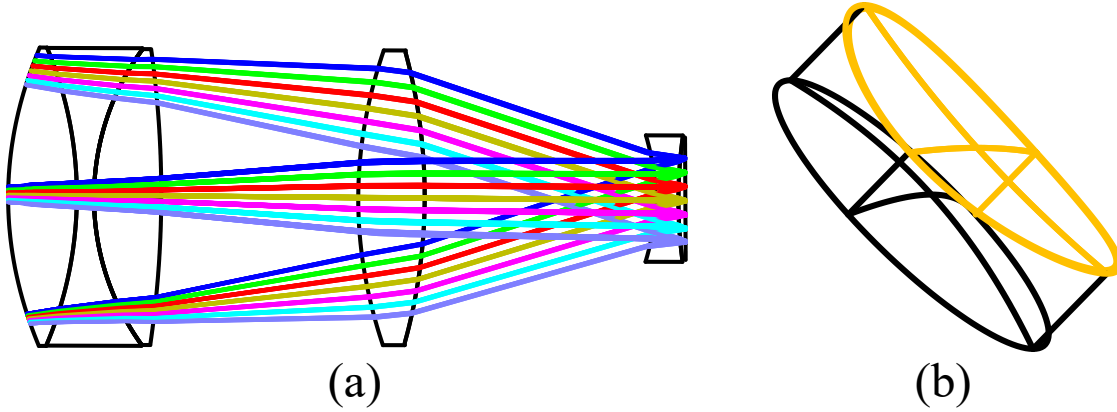


Figure 8: Evolution of the initial structure model for the camera group: (a) Camera lens system; (b) Biconical surface of the field flattener.

further optimization of the whole optical system to improve the optical performance. In the optimization process, we use the diameter of the collimated beam and the size of the spectral imaging area as the constraints. We optimize the line density and the incident angle of the grating while constraining the dispersion angle. The optimization is implemented in ZEMAX [19].

4.3 Design results

The final obtained camera group lens for each channel are shown in Fig. 9, and the final grating parameters are listed in Table 7. The final optimization parameters of the camera group lens in each channel obtained by the optical design software ZEMAX are shown in Table 8 to 11.

4.4 Optical performance

The transmittance is one of the most important metrics of optical performance for the spectrograph system. Since the system has no vignetting effect, we mainly consider two loss factors for the system, i.e. the absorption of glasses

Table 6: Glass material of camera group lens.

Channel	BLUE	RED	NIR	IR
Front group	H-K9LGT	H-QK3L	H-QK3L	H-QK3L
	QF8	H-F2	H-F2	H-F2
	H-QK3L	H-QK3L	H-QK3L	H-QK3L
Rear group	H-K9LGT	H-K9LGT	H-K9LGT	H-K9LGT
Field flatter	F_SILICA	F_SILICA	F_SILICA	F_SILICA

Table 7: **Optimized parameters of the VPH gratings.**

Channel	BLUE	RED	NIR	IR
Wavelength range	360nm-580nm	560nm-740nm	720nm-900nm	877nm-1100nm
Linear density	901 lines/mm	1016 lines/mm	979 lines/mm	792 lines/mm
Incident angle	15.11°	21.432°	24.452°	24.036°
Grating spectral dispersion	11.5318°	10.9880°	10.9359°	10.9199°

Table 8: **Optimization parameters of camera group lens in BLUE channel.**

Element	Material	Curvature Radius(mm)	Thickness (mm)	Conic
Triplet – S1	H-K9LGT	287.430	25.163	-0.954
Triplet – S2	QF8	-1957.749	5.643	0
Triplet – S3	H-QK3L	156.250	54.996	0
Triplet – S4	—	2588.211	188.565	0
Rear – S1	H-K9LGT	223.149	90.000	-0.603
Rear – S2 ^a	—	-443.488	136.757	-2.641
Flat – S1 ^c	F_SILICA	-191.595	5.000	1
Flat – S2 ^c	—	212.592	5.000	0
CCD ^d	—	infinite	—	0

^aAspheric surface coefficients: $\alpha_4 = 3.09E - 009$, $\alpha_6 = -7.72E - 014$.

^bBiconical surface: X Curvature Radius = -182.610 , X Conic = -5 .

^cBiconical surface: X Curvature Radius = infinite, X Conic = 0 .

^dSlit image: slit angle with X axis = 1.680° .

Table 9: **Optimization parameters of camera group lens in RED channel.**

Element	Material	Curvature Radius(mm)	Thickness (mm)	Conic
Triplet – S1	H-QK3L	239.989	48.368	-0.843
Triplet – S2	H-F2	-370.194	11.359	0
Triplet – S3	H-QK3L	250.850	42.000	0
Triplet – S4	—	-787.564	184.632	0
Rear – S1	H-K9LGT	204.668	55.000	-0.192
Rear – S2	—	-832.669	110.718	0
Flat – S1	F_SILICA	-134.887	16.000	-2.786
Flat – S2 ^a	—	317.771	4.985	0
CCD ^b	—	infinite	—	0

^aBiconical surface: X Curvature Radius = 967.739 , X Conic = 0 .

^bSlit image: slit angle with X axis = -0.334° .

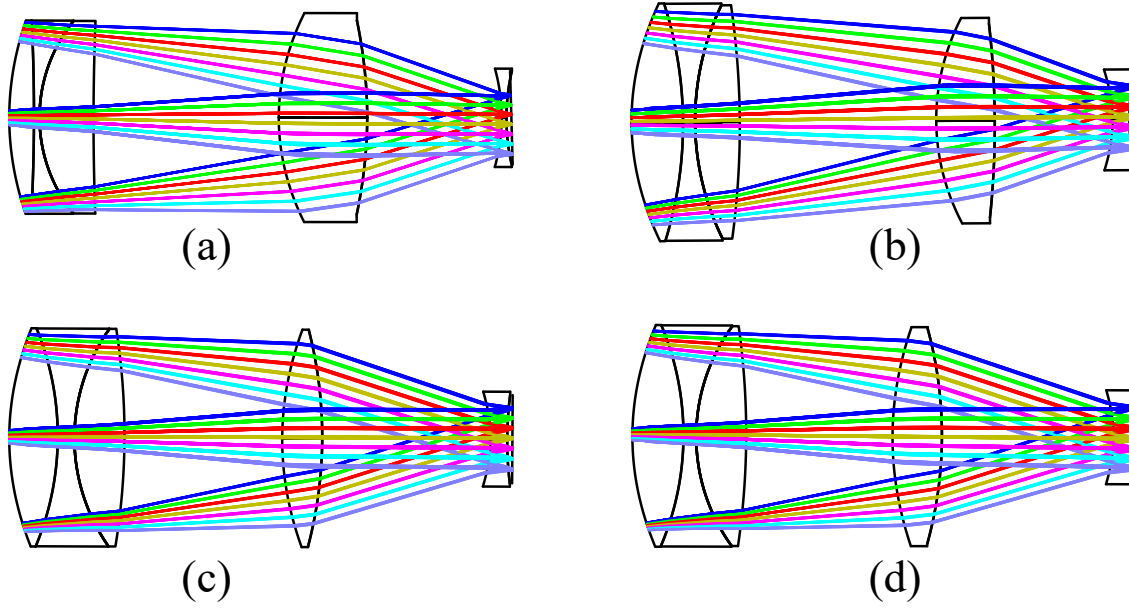


Figure 9: 2D layout of the optimized camera group lens in each channel:(a) BLUE channel; (b) RED channel; (c) NIR channel; (d) IR channel.

Table 10: **Optimization parameters of camera group lens in NIR channel.**

Element	Material	Curvature Radius(mm)	Thickness (mm)	Conic
Triplet – S1	H-QK3L	260.508	46.493	-1.076
Triplet – S2	H-F2	-273.735	15.990	0
Triplet – S3	H-QK3L	180.575	47.999	0
Triplet – S4	—	-659.152	151.243	0
Rear – S1	H-K9LGT	287.219	38.352	-0.886
Rear – S2	—	-413.081	161.364	0
Flat – S1	F_SILICA	-138.478	16.001	-2.586
Flat – S2 ^a		335.936	4.971	0
CCD ^b		infinite	—	0

^aBiconical surface: X Curvature Radius = 603.746, X Conic = 0.

^bSlit image: slit angle with X axis = -0.148° .

and the reflection loss on the optical surfaces. Figure 10 shows the transmittance curves of the four channels. The anti-reflection coatings on the lenses are assumed to have a transmission of 99% in all channels. The result shows that the transmittance meets the requirements given in Table 5.

As shown in Fig. 11, the RMS radius is less than $12.2 \mu\text{m}$ for the RED, NIR, and IR channels, and is less than $13 \mu\text{m}$ for the BLUE channel. The 2D layout of the focal plane is shown in Fig. 12. We can find that the distortions of the spectral images are well controlled(the final optimization parameters of each channel obtained by the optical design software ZEMAX are provided in the appendix). And these results meet the predefined requirements.

5 Tolerance Analysis

To make the spectrometer be friendly to fabrication and alignment, the tolerance budgets are eased in ZEMAX referring to Table 12. A thousand trials of Monte Carlo tolerancing have been performed, and Table 13 lists the five cases which have the biggest negative impact on RMS radius of each channel. Analysis results show that the RMS radius of each channel with 90% confidence is less than $15 \mu\text{m}$ for our proposed error budgets.

Table 11: **Optimization parameters of camera group lens in IR channel.**

Element	Material	Curvature Radius(mm)	Thickness (mm)	Conic
Triplet – S1	H-QK3L	249.801	48.005	-0.979
Triplet – S2	H-F2	-267.096	12.000	0
Triplet – S3	H-QK3L	175.583	47.006	0
Triplet – S4	—	-727.455	137.670	0
Rear – S1	H-K9LGT	299.867	46.438	-1.304
Rear – S2	—	-383.637	161.330	0
Flat – S1	F_SILICA	-135.802	16.000	-2.914
Flat – S2 ^a		320.043	4.845	0
CCD ^b		infinite	—	0

^aBiconical surface: X Curvature Radius = -598.867 , X Conic = 0 .

^bSlit image: slit angle with X axis = 0.474° .

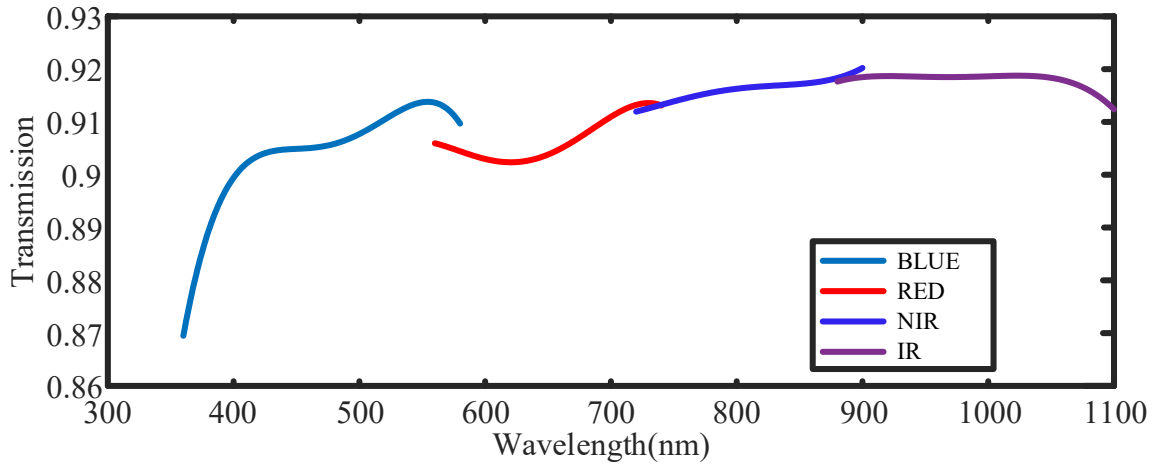


Figure 10: The throughput of the camera group lenses. The blue, red, green and purple curves are for the BLUE, RED, NIR and IR channels respectively.

6 Conclusion

To summarize, we propose a MOFFS system for the wide-field spectroscopic survey telescopes, especially for China's SSST. The proposed design is demonstrated to have superior optical performance with good image quality, high optical throughput, and low cost of glass materials. A brief tolerance analysis of the proposed design indicates a moderate error budget for optical alignment and optical surface quality, which demonstrates its good manufacturability. And we believe that the design ideas, including the calculation of initial structures, optimization procedures of the VPHG parameters as well as the camera groups, can provide a good reference and guidance to researchers for the future instrumentation of such kind of astronomical spectrograph systems.

Funding. National Natural Science Foundation of China (61805088); Science, Technology, and Innovation Commission of Shenzhen Municipality (JCYJ20190809100811375); Key Research and Development Program of Hubei Province (2020BAB121); Fundamental Research Funds for the Central Universities (2019kfyXKJC040); Innovation Fund of WNLO.

Disclosures. The authors declare no conflicts of interest.

References

- [1] Christopher J. Burrows, Pierre Y. Bely, Jon A. Holtzman, S. M. Faber, and Hashima Hasan. The imaging performance of the hubble space telescope. *Astrophysical Journal*, 369(2):L21–L25, 1991.

Table 12: Tolerances setting in ZEMAX of the calculation.

Tolerances	BLUE	RED	NIR	IR
Surface tolerances				
Radius	±0.05mm	±0.05mm	±0.05mm	±0.05mm
Thickness	±0.05mm	±0.05mm	±0.05mm	±0.05mm
Decenter in X	±0.05mm	±0.05mm	±0.05mm	±0.05mm
Decenter in Y	±0.05mm	±0.05mm	±0.05mm	±0.05mm
Tilt in X	±0.01°	±0.05°	±0.03°	±0.05°
Tilt in Y	±0.01°	±0.05°	±0.03°	±0.05°
Element tolerances				
Decenter in X	±0.05mm	±0.05mm	±0.05mm	±0.05mm
Decenter in Y	±0.05mm	±0.05mm	±0.05mm	±0.05mm
Tilt in X	±0.01°	±0.05°	±0.03°	±0.05°
Tilt in Y	±0.01°	±0.05°	±0.03°	±0.05°
Index tolerances				
Index	±0.0003	±0.0005	±0.0004	±0.0005
Abbe	1%	1%	1%	1%

Table 13: Tolerances setting in ZEMAX of the calculation.

Offenders	Increase of RMS radius(μm)
BLUE Channel	
TIND ^a after Triplet – S2	1.5956
TIND after Triplet – S3	1.4958
TIND of the rear lens	0.9982
TETY ^b of the Fold Mirror	0.5327
TETY of the NIR and IR Pass Dichroic	0.5170
RED Channel	
TETY of the Triplet lens	2.7588
TIND after Triplet – S2	2.2484
TETY of the Rear lens	2.1757
TETX ^c of the Rear lens	1.8139
TIND after Triplet – S1	1.7205
NIR Channel	
TIND after Triplet – S2	3.4971
TETX of the Rear lens	2.3165
TIND after Triplet – S3	1.8773
TETY of the Rear lens	1.6681
TIND of the Rear lens	1.4419
IR Channel	
TIND after Triplet – S2	4.1641
TETY of the Rear lens	3.3088
TETX of the Rear lens	2.9817
TIND after Triplet – S3	2.0441
TETY of the Fold Mirror	1.7186

^aTIND:tolerance on index or refraction.

^bTETY:tolerance on element tilt about the y axis.

^cTETX:tolerance on element tilt about the x axis.

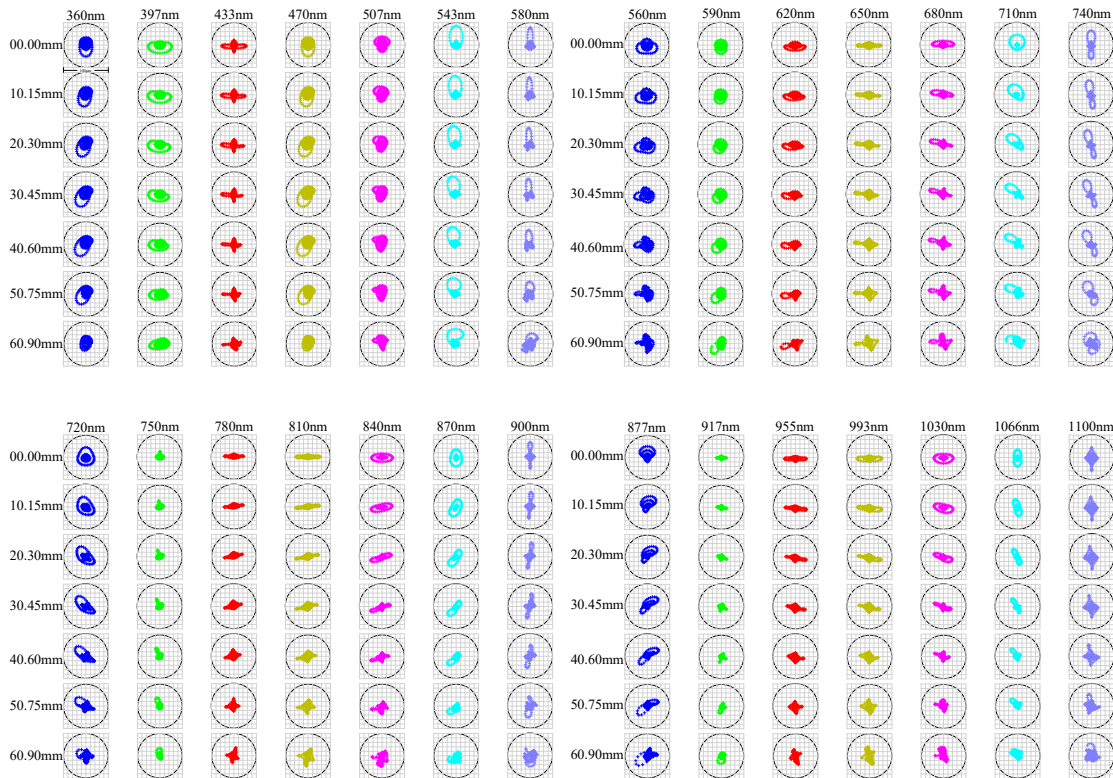


Figure 11: The ray traced spot diagram for the spectrograph.

- [2] Lester J. Kozlowski, Yibin Bai, M. Loose, Atul B. Joshi, Gary W. Hughes, James D. Garnett, J. Anthony Tyson, and Sidney Wolff. Survey and other telescope technologies and discoveries. *Proc. SPIE 4836*, 4836:247–259, 2002.
- [3] Ding Qiang Su, Xiang Qun Cui, and Nanjing University. Two suggested configurations for the chinese space telescope. *Research in Astronomy and Astrophysics*, page 1055–1060, 2014.
- [4] Bernard D. Seery. Next generation space telescope(ngst): Hubble’s scientific and technological successor. *Proceedings of SPIE - The International Society for Optical Engineering*, 4850:170–178, 2003.
- [5] Joan Najita, Beth Willman, Douglas P. Finkbeiner, Ryan J. Foley, and Anja Von Der Linden. Maximizing science in the era of lsst: A community-based study of needed us capabilities, 2016.
- [6] D. N. Spergel, L. Verde, H. V. Peiris, E. Komatsu, M. R. Nolte, C. L. Bennett, M. Halpern, G. Hinshaw, N. Jarosik, and A. Kogut. First year wilkinson microwave anisotropy probe (wmap) observations: Determination of cosmological parameters. *Astrophysical Journal Supplement*, 148(1):175, 2008.
- [7] Z. Ivezić, R. H. Becker, M. Blanton, X. Fan, K. Finlator, J. E. Gunn, P. Hall, R. S. J. Kim, G. R. Knapp, and J. Loveday. Optical and radio properties of extragalactic sources observed by the first and sdss surveys. *Astronomical Journal*, 124(5):2364–2400, 2002.
- [8] Hao Tan and Donglin Ma. Recommended optical system design for the ssst. *Appl. Opt.*, 59(11):3508–3517, Apr 2020.
- [9] Ryker Eads and Roger Angel. 6.5m telescope for multi-object spectroscopy over a 3° field of view. *Applied Optics*, 59(22), 2020.
- [10] DESI Collaboration, Amir Aghamousa, Jessica Aguilar, Steve Ahlen, Shadab Alam, Lori Allen, Carlos Prieto, James Annis, Stephen Bailey, C. Balland, Otger Ballester, Charles Baltay, Lucas Beaufore, Chris Bebek, Timothy Beers, Eric Bell, José Bernal, Robert Besuner, Florian Beutler, and Ying Zu. The desi experiment part ii: Instrument design, 10 2016.

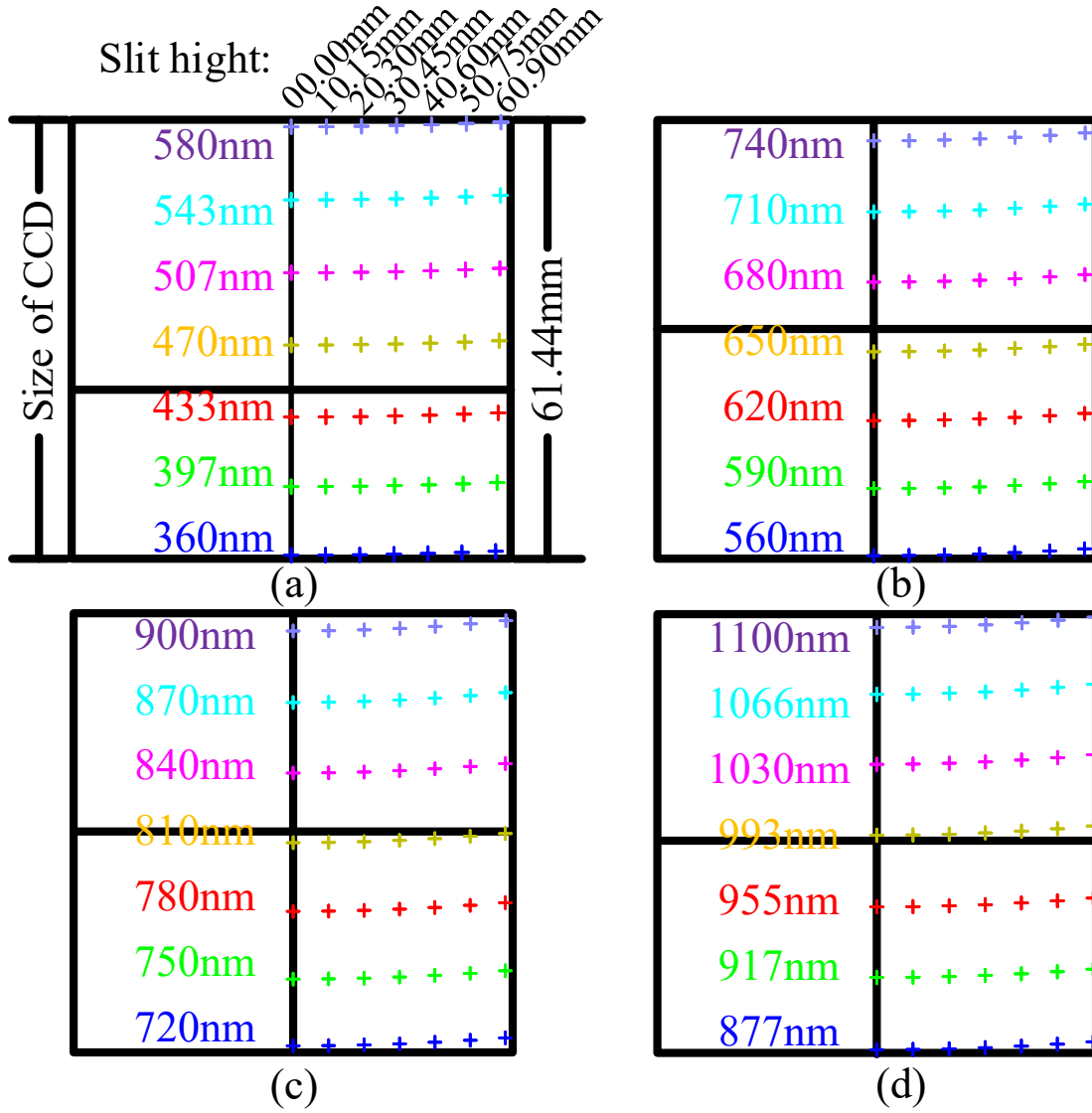


Figure 12: The 2D layout of focal plane of each channel.

- [11] Yan Yunxiang, Wang Gang, Sun Weimin, Luo A-Li, Ma Zhenyu, Li Jian, and Wang Shuqing. A modified method for determining the focal ratio degradation and length properties of optical fibres in astronomy. *Monthly Notices of the Royal Astronomical Society*, page 1669–1687, 2016.
- [12] Jesulino Bispo Dos Santos, Antonio Cesar De Oliveira, James Gunn, Ligia Souza De Oliveira, Marcio Vital De Arruda, Bruno Castilho, Clemens Darvin Gneiding, Flavio Felipe Ribeiro, Graham Murray, and Daniel J. and Reiley. Studying focal ratio degradation of optical fibers for subaru prime focus spectrograph. *Proc. SPIE 9151*, page 915150, 2014.
- [13] Lisa Crause, Matthew Bershady, and David Buckley. Investigation of focal ratio degradation in optical fibres for astronomical instrumentation. *Proc. SPIE 7014*, page 70146C, 2008.
- [14] Lawrence Ramsey. Focal ratio degradation in optical fibers of astronomical interest, 01 1988.
- [15] V.LAPERRE, D.SOLER, and P.GODEFROY. Feasibility study of bigboss spectrograph, 2013.
- [16] Warren J. Smith. Objective of the petzval type with field flattener and three or more positive elements. *U. S. patent*, pages 3,255,664, 1966.
- [17] W. J. Smith. Modern lens design. *McGraw-Hill*, 1992.

- [18] Bertram Aichtner. Handbook of optical systems volume 4: Survey of optical instruments, 2008.
- [19] <https://www.zemax.com/>.